ChemCatChem

ChemCatChem
Chemistry Europe
European Chemical Societies Publishing

RESEARCH ARTICLE OPEN ACCESS

Redirecting a Fungal Quercetin 2,3-Dioxygenase Toward Artificial Flavonols

Michael Kotik[1] | Natalia Kulik[2] | Stanislav Musil[3] | Petr Halada[4] | Lucie Petrásková[1] | Andrea Ramundo[5,6] | Tatsiana Charnavets[7] | Martina Hurtová[1] | Vladimír Křen[1] | Kateřina Valentová[1]

[1]Laboratory of Biotransformation, Institute of Microbiology, Czech Academy of Sciences, Vídeňská 1083, Prague, Czech Republic | [2]Laboratory of Photosynthesis, Centre Algatech, Institute of Microbiology, Czech Academy of Sciences, Třeboň, Czech Republic | [3]Institute of Analytical Chemistry, Czech Academy of Sciences, Veveří 97, Brno, Czech Republic | [4]Institute of Microbiology, BIOCEV, Czech Academy of Sciences, Průmyslová 595, Vestec, Czech Republic | [5]Department of Chemistry, Faculty of Science, Masaryk University, Brno, Czech Republic | [6]RECETOX, Faculty of Science, Masaryk University, Brno, Czech Republic | [7]Institute of Biotechnology, BIOCEV, Czech Academy of Sciences, Průmyslová 595, Vestec, Czech Republic

Correspondence: Michael Kotik (kotik@biomed.cas.cz)

Received: 9 December 2025 | **Revised:** 4 February 2026 | **Accepted:** 3 March 2026

Keywords: biotransformation | enzyme engineering | enzyme evolution | structure-activity relationships | substrate specificity

ABSTRACT

A novel quercetin 2,3-dioxygenase from *Penicillium chrysogenum*, following biochemical characterization, served as the starting point for reshaping the substrate-binding cavity to alter its substrate specificity. Using a rational engineering strategy supported by computational predictive tools, we achieved high activity toward specific artificial flavonols. In all generated variants, amino acids were replaced with residues that naturally occur at the selected positions in homologous enzymes. Two variants with enlarged substrate-binding cavities exhibited improved activity toward bulkier substrates. In particular, the Y55F-F134L-M143L variant showed 20- to 1750-fold higher activity toward flavonol compounds with phenyl-based substitutions at position C-8. Conversely, one variant with a smaller substrate-binding cavity showed 15-fold higher activity toward the smaller flavonol 3,7-dihydroxyflavone. The procedure described here has implications for engineering metalloenzymes to alter their substrate specificity toward novel compounds.

1 | Introduction

Flavonols are abundant secondary metabolites in many plants and are important constituents of the human diet [1]. They can also serve as sources of carbon and energy for various microorganisms [2]. The flavonol quercetin (compound **1**, Figure 1), for example, is a widely used dietary supplement due to its beneficial effects on human health, such as reducing oxidative stress, and its anti-inflammatory, antibacterial, and antiviral activities, as well as its protection against cardiovascular diseases and positive effects on the treatment of certain cancers [3]. In addition, compound **1** and its natural or semi-synthetic derivatives can enhance the activity of various antibiotics, thereby combating resistant pathogenic strains [4]. For example, substituted anilines incorporated into the flavonol core (see compounds **17** and **18**) have been shown to reduce antibiotic resistance in *Staphylococcus aureus* [5].

Understanding and controlling the enzymatic degradation of artificial flavonols is essential for evaluating their metabolic fate and obtaining defined cleavage products needed for biological and pharmacological studies. In addition to their nutritional and pharmacological relevance, the enzymatic C-ring cleavage of flavonols is a key biochemical transformation that governs detoxification and various other, not yet fully understood, intracellular processes through their enzymatic reaction products, including the release of CO [6–9].

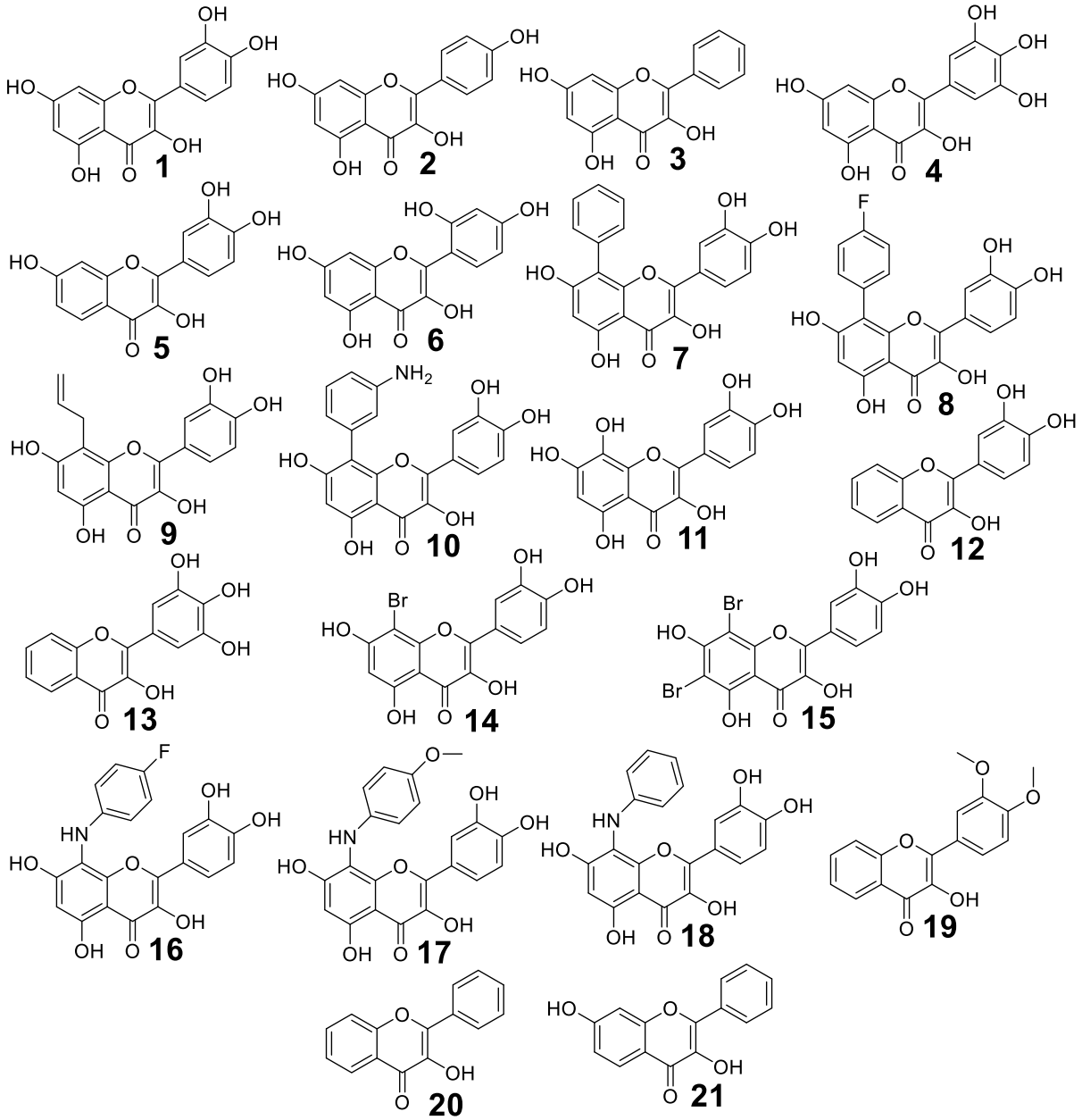

FIGURE 1 | Structures of compounds tested as substrates. Natural flavonols are: **1** (quercetin), **2** (kaempferol), **3** (galangin), **4** (myricetin), **5** (fisetin), **6** (morin), and **11** (gossypetin). The general structure of flavonols is represented by compound **20** (3-hydroxyflavone).

The C-ring fission of natural flavonols is mediated by microbial quercetin 2,3-dioxygenases (QueDs) and by several pirins, which are widely distributed in mammals and plants and were first described as transcription regulators [10]. Both QueDs and the pirins studied so far act as nonheme metalloenzymes on various flavonols, exhibiting a molecular oxygen-dependent reaction mechanism that generates a depside and CO as reaction products (Scheme 1a) [11]. Milestones in QueD research include the elucidation of their X-ray structures and reaction mechanism [12–17]. In QueDs, the flavonol substrate binds to the metal center in a monodentate arrangement through the oxygen atom at C-3 of the flavonol (Scheme 1b).

This study is the first to determine the structural requirements in QueD for high ring-cleavage activity toward artificial flavonols, in the context of developing flavonol-based therapeutics for managing antibiotic resistance. Authentic standards are also needed to identify and quantify potential depside products generated in human tissues or by microbiota in the human gut through pirin- or QueD-mediated breakdown of natural and artificial flavonols.

QueD from *Penicillium chrysogenum* (*Pc*QueD) was selected because it shows high activity toward multiple natural flavonols, is readily produced in a eukaryotic expression system, and shares substantial sequence identity with characterized QueDs. These features make *Pc*QueD a suitable and experimentally tractable model for rational engineering of the substrate-binding cavity.

In addition to QueDs and pirins, there are a few other metalloenzymes with similar basic scaffold structures [18]. In this context,

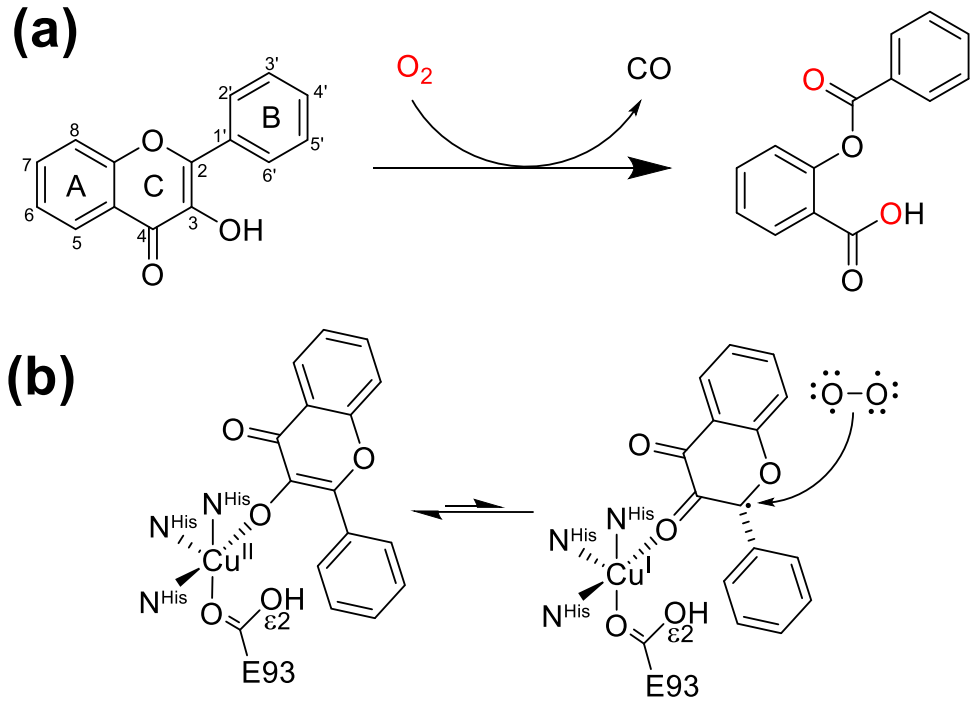

SCHEME 1 | (a) Reaction catalyzed by QueD with a flavonol as substrate and molecular dioxygen as co-substrate, resulting in the formation of CO and a depside. Only the flavonol backbone is shown with its ring nomenclature and substituent numbering. (b) After binding to the active site, the flavonol coordinates to the copper ion as a monodentate ligand via its oxygen atom at C-3. The copper center forms a coordination complex with three histidine side chains (H86, H88, and H132) and the carboxyl group of E93. In the following steps, the reaction mechanism involves the formation of a flavonoxy radical–Cu^{+} valence tautomer, which reacts with the diradical oxygen molecule to generate peroxide and endo-peroxide reaction intermediates (not shown) [16].

gentisate and salicylate 1,2-dioxygenases should be mentioned. These are Fe(II)-dependent ring-cleaving dioxygenases that catalyze the oxidative cleavage of one carbon–carbon bond in the substrate [19, 20].

This enzyme engineering study aimed to alter the substrate scope of a QueD by targeting the substrate-binding cavity, either by removing steric hindrances to accommodate larger substrates or by filling the cavity with larger residues when smaller substrates are bound. Strategies for reshaping catalytic cavities to change substrate specificity have been successfully pursued [21–25]. However, it should be noted that enzyme catalysis depends on a delicate balance of many interactions and factors not captured by molecular docking simulations alone [26]. Due to the complexity of enzyme-catalyzed processes, improvements in turnover numbers for enzyme variants are often moderate, typically ranging from 1.5- to 10-fold [27]. There are, however, notable exceptions with activity improvements of a hundredfold or more, mainly achieved through enzyme engineering approaches based on directed evolution or machine learning [21, 28].

Reports on the manipulation of dioxygenase activities by enzyme engineering are rather sparse. Nazmi and coworkers increased the specific activity of a (chloro-)catechol 1,2-dioxygenase for catechol and its derivatives by up to 5-fold, truncating the non-conserved C-terminus, which has been shown to interfere with the substrate-binding cavity [29]. The substrate-binding cavity of another catechol 1,2-dioxygenase was redesigned by focusing on two residues, avoiding clashes in the binding of catechol derivatives with substituents at C-4. Here, improvements in k_{cat} and k_{cat}/K_M values were found to be 2- and 5-fold, respectively [30].

As far as the enzyme engineering of structurally similar dioxygenases is concerned, three works should be mentioned. The substrate spectrum of the aforementioned salicylate 1,2-dioxygenase, with its broad specificity, was narrowed by a single point mutation in the active-site cavity, resulting in an enzyme that accepts only gentisate [20]. Conversely, introducing the reverse mutation in a specific gentisate 1,2-dioxygenase broadened the substrate spectrum to include gentisate and monohydroxylated substrates, such as salicylate and 1-hydroxy-2-naphtholate, mimicking a salicylate 1,2-dioxygenase with broad specificity. However, the k_{cat}/K_M values for the new substrates did not exceed 6% of the corresponding gentisate-based value [31]. Third, the Mn-dependent QueD from *Bacillus subtilis* has been evolved into an enzyme that accepts nickel or manganese ions in the active site and shows good specific activities toward compounds **1** and **2** in both enzyme forms [32].

In this study, we successfully modified the substrate-binding cavity of our model enzyme, *Pc*QueD, through rational site-directed engineering. This produced enzyme variants with markedly enhanced catalytic efficiencies toward nonnatural flavonols that are either smaller or larger than compound **1**. The small number of amino acid substitutions introduced indicates that our evolution-inspired engineering approach is suitable for straightforward modification of

the substrate spectrum while maintaining high enzyme activity.

2 | Results and Discussion

2.1 | Cloning

Seven peptides of wild-type *Pc*QueD, co-purified during the purification of *Pc*Rut from *Penicillium chrysogenum* CCF 1269 [33], were obtained by trypsin treatment of an SDS-PAGE protein band and subsequently characterized by MALDI-TOF mass spectrometry (Table S1). Amplification attempts with peptide-derived degenerate primers were not successful (Table S2). However, we were able to amplify the full-length *Pc*QueD-encoding gene using specific primers that were derived from the noncoding regions outside the locus Pc16g11830 of *Penicillium rubens* Wisconsin 54-1255 (AM920431.1) (Table S2). The amplified chromosomal DNA segment was found to be identical to the nucleotide sequence of the above-mentioned locus. A comparison of chromosomal DNA-derived and mRNA-derived sequences revealed the presence of a 52-bp long intron, resulting in a protein sequence that was identical to CAP93853.1 and served as the basis for amino acid numbering.

2.2 | Characterization of Recombinant Wild-Type *Pc*QueD

After purification of His-tagged *Pc*QueD by immobilized metal chelate affinity chromatography (IMAC; Figure S1), SDS-PAGE analysis indicated the presence of glycan chains bound to the protein, resulting in smearing of the protein bands (Figure S2). Glycosylation of *Pc*QueD was confirmed by mobility shift experiments using the endoglycosidase PNGase F for glycan removal (Figure S3).

A plateau region with high *Pc*QueD activities was found between pH 3.5 and 7.5. Beyond these pH values, a loss of enzyme activity was observed (Figure S4).

ICP-MS analysis of purified native *Pc*QueD showed that the total metal occupancy was 113% per polypeptide chain, with copper accounting for 95.8% per chain. Traces of bound Mn^{2+}, Zn^{2+}, and Ni^{2+} were also detected (Table S3). These results are consistent with the finding that fungal QueDs are mononuclear copper enzymes [12, 34]. After chelation of the enzyme-bound copper, the activity of apo-*Pc*QueD decreased to a few percent of the native enzyme's activity (Figure S5). Reconstitution with Cu^{2+} ions restored enzyme activity, while reactivation with other transition metals was less effective and did not exceed 17% of the native enzyme's activity (Figure S5).

The quaternary structure of native *Pc*QueD was determined by mass photometry to be dimeric for both the apoenzyme and the copper-reconstituted enzyme (Figure S6), consistent with the quaternary structures determined for QueDs from *Aspergillus japonicus*, *Bacillus subtilis*, and *Streptomyces* sp. [18].

Circular dichroism (CD) spectra in the far- and near-UV regions of apo and reconstituted *Pc*QueD indicated very similar secondary structure contents and similar spatial environments of aromatic residues (Figures S7 and S8). However, the data may suggest an exchange of a small proportion of antiparallel β-sheet for α-helix upon metal reconstitution of apo-*Pc*QueD (Figure S7; Table S4). Similarly, the near-UV CD data may indicate slight structural rearrangements around aromatic residues upon metal reconstitution.

TABLE 1 | Apparent steady-state kinetic parameters of recombinant wild-type *Pc*QueD arranged according to specificity constants.[a]

Compound	K_M [μM]	k_{cat} [sec^{-1}]	k_{cat}/K_M [$\mu M^{-1}\ s^{-1}$]	K_i [μM]
2	6.3 ± 0.9	200.1 ± 13.9	31.6	149
6	8.8 ± 2.5	128.5 ± 19.4	14.7	82
1	6.0 ± 0.6	59.5 ± 1.7	9.9	—
14	6.3 ± 1.8	20.7 ± 2.3	3.3	132
15	7.4 ± 1.8	17.5 ± 2.1	2.4	114
11	32.6 ± 2.7	62.9 ± 2.1	1.9	—
3	17.1	27.5	1.6	n.d.[b]
5	39.8 ± 15.3	51.4 ± 15.1	1.3	34
4	58.4 ± 12.2	62.2 ± 10.1	1.1	56
12	26.5 ± 3.0	3.59 ± 0.15	0.14	—
19	15.8	1.31	0.08	n.d.[b]
21	22.0	0.42	0.02	n.d.[b]
13	132.8	0.36	0.003	n.d.[b]
20	2816	5.5	0.002	n.d.[b]

[a]Purified native enzyme was used as the catalyst. Reaction conditions: 22°C, 50 mM MES (pH 5.5; aerated buffer), 3% dimethyl sulfoxide. The K_i values are provided for informational purposes only. Unless otherwise specified, nonlinear regression analysis was performed using the Michaelis-Menten equation with a substrate inhibition term [38]. See Figure S9 for the corresponding graphs.

[b]Due to solubility issues at higher substrate concentrations, kinetic parameters were obtained from Lineweaver-Burk plots (Figure S9); n.d., not determined.

Artificial intelligence-based structure modeling indicated that wild-type *Pc*QueD is structurally very similar to the experimentally determined structure of QueD from *Aspergillus japonicus* (C_α RMSD of 0.703 Å over 324 aligned residues with 62.7% sequence identity; Figure 2).

The carbon monoxide released during *Pc*QueD-mediated conversion of compound **1**, labeled with ^{13}C at position C-3, was found to originate solely from this carbon atom (Scheme 1; Table S5). This finding is consistent with earlier results of manometric experiments performed with rutin (quercetin rutinoside) labeled with ^{14}C at position C-3 of the aglycone and culture filtrate of *Aspergillus niger* as the enzyme source [36]. Thus, the QueD-mediated reaction consumes one mole of oxygen per mole of flavonol, generating one mole of carbon monoxide (Scheme 1a) [37].

The substrate spectrum of *Pc*QueD was analyzed using a range of natural and synthetic flavonols (Table 1 and S6). The best substrates were the naturally occurring compounds **2**, **6**, and **1** with

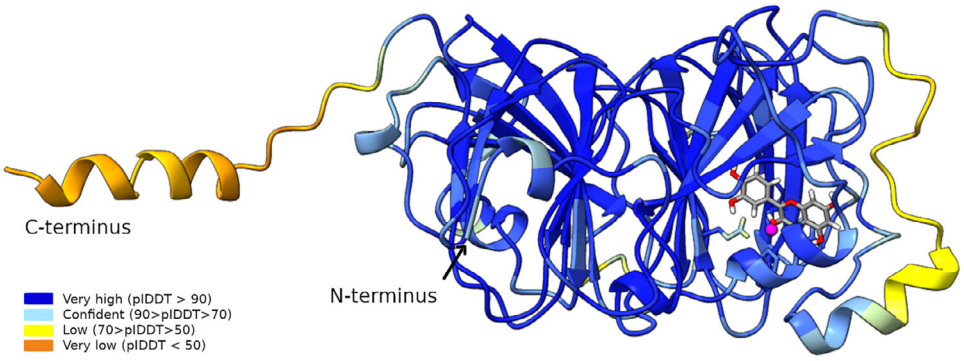

FIGURE 2 | Ribbon diagram of the wild-type *Pc*QueD monomer. The structure is based on a representative model of *Pc*QueD generated using the AlphaFold 3 server. The protein consists of two β-barrel folds, that is, two cupin domains, with the N-terminal domain containing a divalent copper ion (shown in magenta) coordinated by H86, H88, H132, E93, and bound compound **1** [14]. Coloring reflects the confidence of the structure prediction using pLDDT (predicted local distance difference test) [35]. The most flexible regions are the polypeptide segment 176–188, located near the active site entrance, and the C-terminal His-tag.

apparent k_{cat}/K_M values of 10–32 μM^{-1} s^{-1}. The transformation of compound **1** by *Pc*QueD produced a reaction product whose NMR-derived structure was fully consistent with previously published NMR data (Figures S10 and S11) [39]. The poorest substrates were the artificial compounds **7**, **8**, **10**, **12**–**13**, and **16**–**21**. In contrast, the natural flavonols **3**, **4**, **5**, and **11**, as well as the quercetin derivatives **14** and **15** with additional small substitutions at C-6 and C-8, showed intermediate k_{cat}/K_M values of 1.1–3.3 μM^{-1} s^{-1}. Compound **9**, which resembles prenylated quercetin (Table S6), also exhibited intermediate activity. Higher O_2 concentrations increased the enzyme activity for compound **1**; in O_2-saturated buffer, we observed a 1.8-fold increase in k_{cat}, while the K_M value remained unchanged, suggesting that O_2 was not saturating in the aerated buffer (Figure S12; Table S7). The substrate ranges of *Pc*QueD and QueD from *Penicillium olsonii*, which share 81.3% sequence identity, were similar regarding the best substrates, compounds **2** and **1**. However, in stark contrast to *Pc*QueD, no activity was reported for compound **6** with the latter enzyme [34], indicating structural differences in the binding pocket for ring B of the substrate, as supported by molecular docking analysis (Figure S13).

2.3 | Selection of Sites for Mutagenesis

The strategy for amino acid replacement was initiated by aligning ninety similar sequences from the NCBI database with sequence identities of 26.9%–100% relative to *Pc*QueD (Table S8), followed by structure modeling. After molecular docking of compound **1** into the binding pocket of modeled *Pc*QueD, specific amino acids were selected and replaced with naturally occurring amino acids at those positions based on multiple sequence alignment of homologous QueDs (Figure S14). This alignment served as an evolutionary filter for mutational robustness, selecting likely permissible amino acid substitutions in structurally similar QueDs. See Table S9 for the degrees of conservation at the sites selected for mutation. To improve binding of bulkier substrates (compounds **7**, **8**, **16**, **17**, and **18**), we selected residues with high collision potential and replaced them with residues that have smaller accessible surfaces to reduce clashes between the enzyme and the bound substrate (e.g., Phe → Leu) [40]. This resulted in two enzyme variants: Mut1/2, Y55V/F–F134L–M143L. In contrast, for smaller substrates, such as compounds **3**, **20** and **21**, certain residues were replaced with residues that have larger accessible surface areas to fill the empty space (e.g., Thr → Leu), resulting in two mutants: Mut3/4, T73L–M143F–G145A–V147I/F. All newly introduced amino acids were hydrophobic (Figure 3a). A 100-ns molecular dynamics simulation of wild-type *Pc*QueD and its mutants revealed that the mutations likely introduced only very small structural alterations. Mut1 was found to have the most flexible residues at the mutated sites of all investigated enzymes (Figure S15).

The thermal unfolding data for *Pc*QueD and its variants showed that the mutant enzymes had lower thermostabilities than wild-type *Pc*QueD, which had melting temperatures of 62°C in the activity-based assay and 70°C in the fluorescence-based assay. The least thermostable enzyme was Mut2, with melting temperatures of 57°C in the activity-based assay and 63°C in the fluorescence-based assay (Figure S16).

2.4 | Substrate Specificities and Catalytic Constants of *Pc*QueD Variants

Using the above-mentioned strategy based on multiple sequence alignment and molecular docking, we designed, produced, and purified four *Pc*QueD variants intended for higher activity toward either flavonols with substitutions at C-8 (Mut1 and Mut2) or smaller flavonols (Mut3 and Mut4) (Figures S17–S23). According to the molecular docking results, Mut1 and Mut2 should allow binding of compounds **8**, **16**, and **18** in their substrate-binding pockets, in contrast to wild-type *Pc*QueD. Compound **21**, which lacks three hydroxyls in comparison with compound **1**, was predicted to bind to all enzyme variants and wild-type *Pc*QueD with very similar binding energies (Figure 4).

A detailed analysis of the docking results revealed a high collision potential between the additional phenyl-based substituent of compounds **16** and **18** and residues Y55 and F134 in the substrate-binding pocket of wild-type *Pc*QueD (Figure 3b). In contrast, the simulated binding of compound **16** to Mut2 indicated favorable

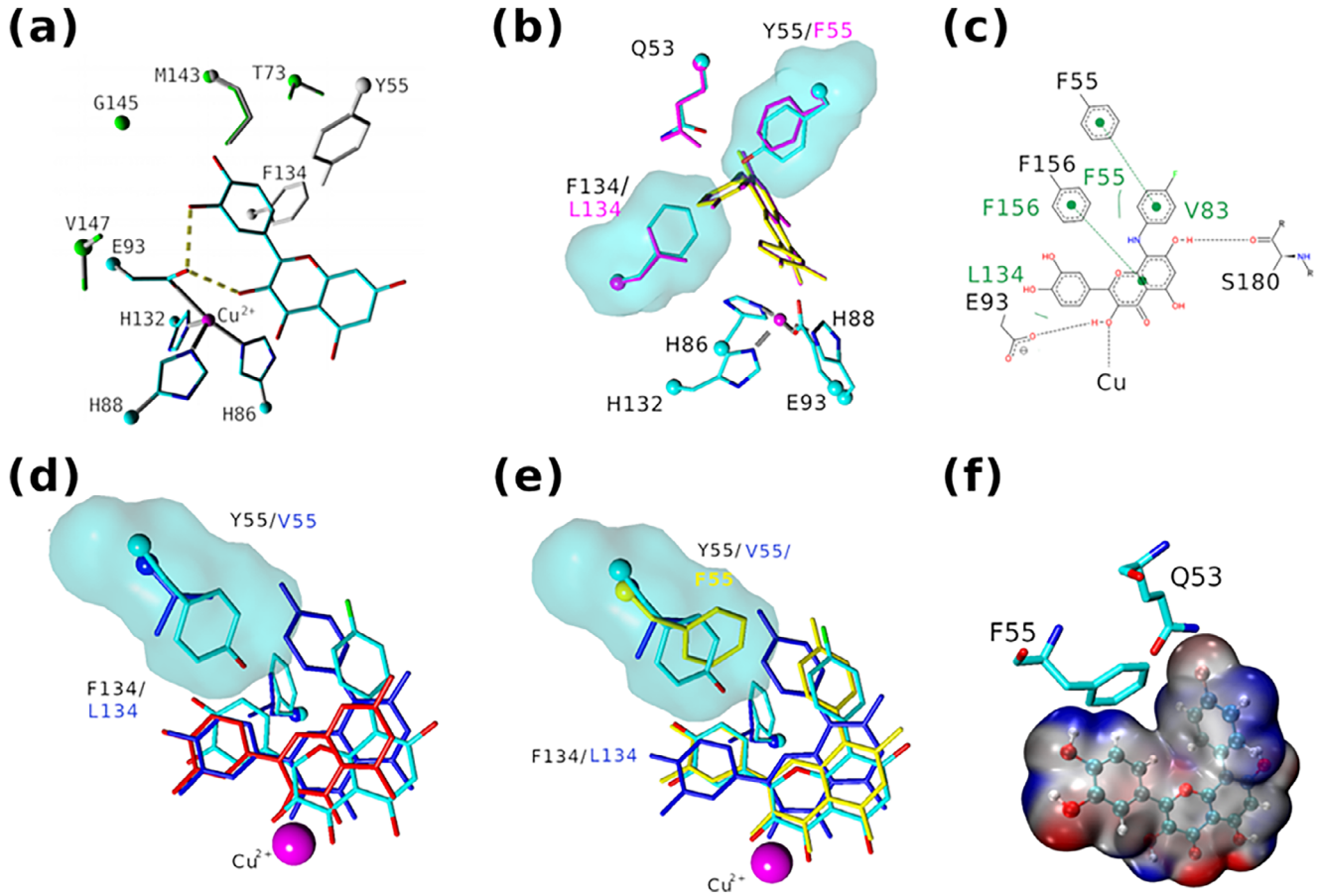

FIGURE 3 | (a) Substrate-binding cavity of wild-type *Pc*QueD with docked compound **1**. Conserved copper-coordinating residues are H86, H88, H132, and E93. Wild-type amino acids replaced in the mutants are shown in gray (Mut1/2: Y55V/F–F134L–M143L) and in green (Mut3/4 T73L–M143F–G145A–V147I/F). C_α atoms are shown as spheres, and hydrogens are omitted. (b) Poses of compounds **16** (magenta) and **18** (yellow) docked to the substrate-binding cavity of Mut2 (residues in magenta) are shown together with the corresponding residues of wild-type *Pc*QueD (colored by element: cyan for carbon, red for oxygen, and blue for nitrogen) after structural alignment of both proteins. (c) Interactions formed between docked compound **16** and Mut2 as displayed by PoseView: hydrogen bonds and electrostatic interactions are shown as black dashed lines; green lines and green labels indicate hydrophobic interactions; π-stacking interactions are depicted as connected filled green circles. (d) Poses of compound **8** (in blue and element colors) docked to the substrate-binding cavities of Mut1 (blue) and wild-type *Pc*QueD (element color) are shown. Compound **1** docked to wild-type *Pc*QueD is shown in red. (e) The poses of compound **8** (blue, yellow, and element colors) docked to Mut1 (blue), Mut2 (yellow), and wild-type *Pc*QueD (element color), respectively, are shown. (f) Electrostatic potential mapped for compound **8** docked to Mut2, with negative potential in red and positive potential in blue. A hydrogen bond may form between the fluorine atom and the closely positioned polar amide group of Gln53 with a distance of 2.5–3.4 Å.

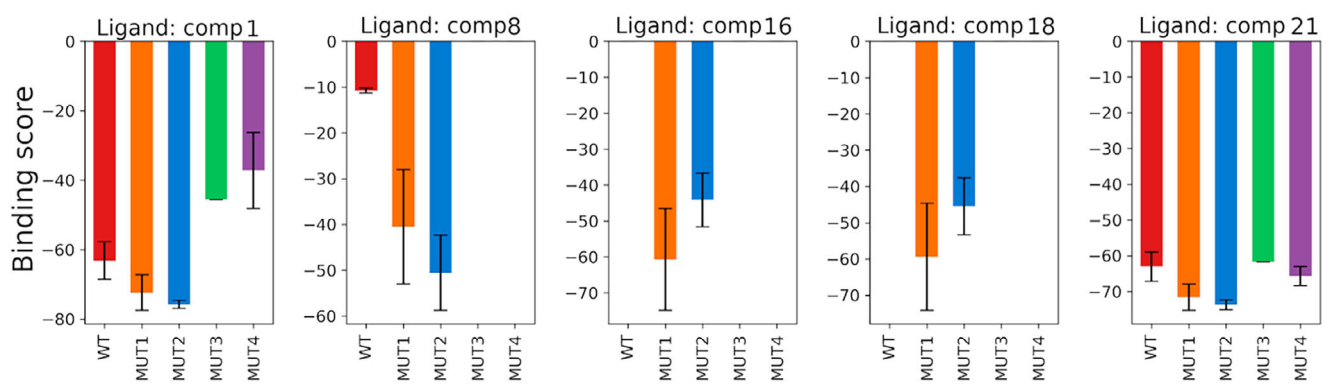

FIGURE 4 | Ligand binding energies of compounds **1**, **8**, **16**, **18**, and **21** for wild-type *Pc*QueD (WT) and its variants Mut1, Mut2, Mut3, and Mut4. The averaged data and standard deviations are based on molecular docking simulations using several representative AlphaFold 3 enzyme models.

hydrophobic and π-stacking interactions, as well as hydrogen bonds (Figure 3c). Differences in the binding poses of compound **8** in the substrate-binding pockets of Mut1, Mut2, and wild-type *Pc*QueD presumably explain part of the substantial differences in activities among the three enzymes. The important role of residue 55 in accommodating compound **8** is highlighted (Figure 3d,e). Calculations of electrostatic potentials revealed a possible additional positive interaction between the side chain of Q53 and the fluorine atom of docked compounds **8** and **16** in Mut2 (Figure 3f).

The X-ray structure of QueD from *Aspergillus japonicus*, anaerobically complexed with compound **1**, revealed distances of about 2.3 Å between the oxygen atom at C-3 of bound **1** and the copper center, and 2.7 Å between HO3 of **1** and $O_{\varepsilon 2}$ of the copper-coordinating Glu, suggesting close interactions that assist in forming the enzyme-substrate complex (Scheme 1b) [14]. In the modeled enzyme-substrate complexes of experimentally validated active enzyme-substrate combinations, nearly all distances were within the range of 2.1–2.6 Å (Table S10), indicating likely productive substrate poses. Although the distances in low-activity combinations were often higher, the difference in distances between active and low-activity complexes was not statistically significant (Table S11).

The four *Pc*QueD variants were tested for their specific activities with substrates **1**–**21**. For Mut1 and Mut2, which were designed to improve binding of bulkier flavonols, Mut2 showed the greatest increases in activity, with 725- to 1750-fold higher specific activities for compounds **8**, **16**, and **18** compared with wild-type *Pc*QueD. Eliminating substrate-induced collisions with residues in the substrate-binding pocket led to much higher activities of Mut2 toward bulky flavonols (Figure 5a). In terms of absolute specific activities, Mut2 achieved fairly high values of 2.2–2.9 s^{-1} at 30 μM substrate concentrations for compounds **7**, **8**, **16**, and **18** in aerated buffer (Table S12). Notably, compared with wild-type *Pc*QueD, the activity of Mut2 toward the natural flavonol **1** decreased from 50 to 2.0 s^{-1}. The much higher activities of Mut2 toward compounds **8**, **16**, and **18** enabled determination of their apparent Michaelis-Menten parameters, which ranged from 13.5 to 26.0 μM for K_M and 3.8 to 7.2 s^{-1} for k_{cat} (Table S13; Figure S24). Under O_2 saturation, the apparent kinetic parameters changed. For compound **8**, high oxygen conditions alleviated the strong substrate inhibition observed in aerated buffer. For compound **16**, the apparent k_{cat} value more than doubled in the presence of O_2 saturation. This again indicates the absence of O_2-saturating conditions in the aerated buffer. For both compounds, the specificity constant k_{cat}/K_M increased under high oxygen concentrations (Table S13; Figure S25). The mass spectrometry data for the products matched expectations (Figure S26).

Of the two variants designed to reduce empty space in the substrate-binding pocket, only Mut3 showed notable activity, specifically toward compounds **1**, **3**, and **21**, with specific activities exceeding 3 s^{-1} (Table S12). Compared with wild-type *Pc*QueD, a 15-fold improvement in activity was observed only for compound **21** (Figure 5b). This does not agree with the molecular docking results, which identified favorable binding poses for all investigated enzymes (Figure 4). However, close inspection of the poses of compound **21** revealed substantial differences between wild-type *Pc*QueD and Mut3, with hydrogen bonds, electrostatic, hydrophobic, and π-stacking interactions likely stabilizing the complex (Figure S27). Regarding the very low activity of Mut4 with all tested compounds, we conclude that the combined amino acid substitutions in this variant likely created a substrate-binding pocket incompatible with activity, even for the smallest flavonols, compounds **20** and **21**. We speculate that one reason for the lack of activity toward compound **21** is the distance between HO3 and $O_{\varepsilon 2}$ of catalytic E93, which exceeds a critical limit in Mut4 (Table S10). At this point, we must emphasize that ligand binding is a prerequisite for enzyme catalysis. However, this does not guarantee high activity for two reasons: (1) a key aspect of catalysis in naturally evolved enzymes is stabilization of the transition state with relatively weak substrate binding in the ground state, information not accessible by molecular docking [41, 42]; and (2) enzyme-based catalytic processes are very complex, far more so than simply addressing ligand binding [26]. The molecular docking data of compound **21** illustrates the limits of docking-based ranking and underscores the importance of experimental validation.

Remodeling substrate-binding cavities of enzymes with large positive effects on their substrate specificity has recently been described in a few reports that used more challenging methods, such as directed evolution or gene library construction [21, 22].

In our engineering project, we used a rational approach with computational predictive tools based on protein structure modeling, molecular docking of substrate ligands, and sequence-based information from homologous enzymes. This approach proved viable, identifying key sites in the substrate-binding pocket to be altered by site-directed mutagenesis and predicting a small number of enzyme variants with likely tolerated substitutions selected from QueDs with a common evolutionary history. Three of the four introduced sets of mutations redirected the enzyme toward novel substrates by reshaping the substrate-binding pocket to better accommodate the new substrates. This highlights the high probability of enzyme improvement using our approach, which is based on evolutionarily selected, likely QueD-compatible alternative residues. We suggest that our approach is especially suited for enzymes that require eukaryotic hosts for expression, as in this case directed evolution and saturation mutagenesis are much more difficult to perform than with prokaryotic hosts.

3 | Conclusion

By introducing mutations in the substrate-binding cavity, we significantly increased the activity of our model enzyme, a fungal quercetin 2,3-dioxygenase, toward specific artificial flavonols. Using an AlphaFold 3 model of the enzyme, our strategy involved molecular docking of compound **1**, identifying key amino acids in the substrate-binding cavity whose substitution would improve binding of novel artificial flavonols, and selecting amino acids that are evolutionarily conserved at these positions in homologous enzymes, considering the requirement to bind either smaller or bulkier flavonols. Two variants with enlarged substrate-binding pockets exhibited up to a 1750-fold increase in activity toward bulkier flavonols with phenyl-based substitutions at C-8. In contrast, one variant with a smaller substrate-binding

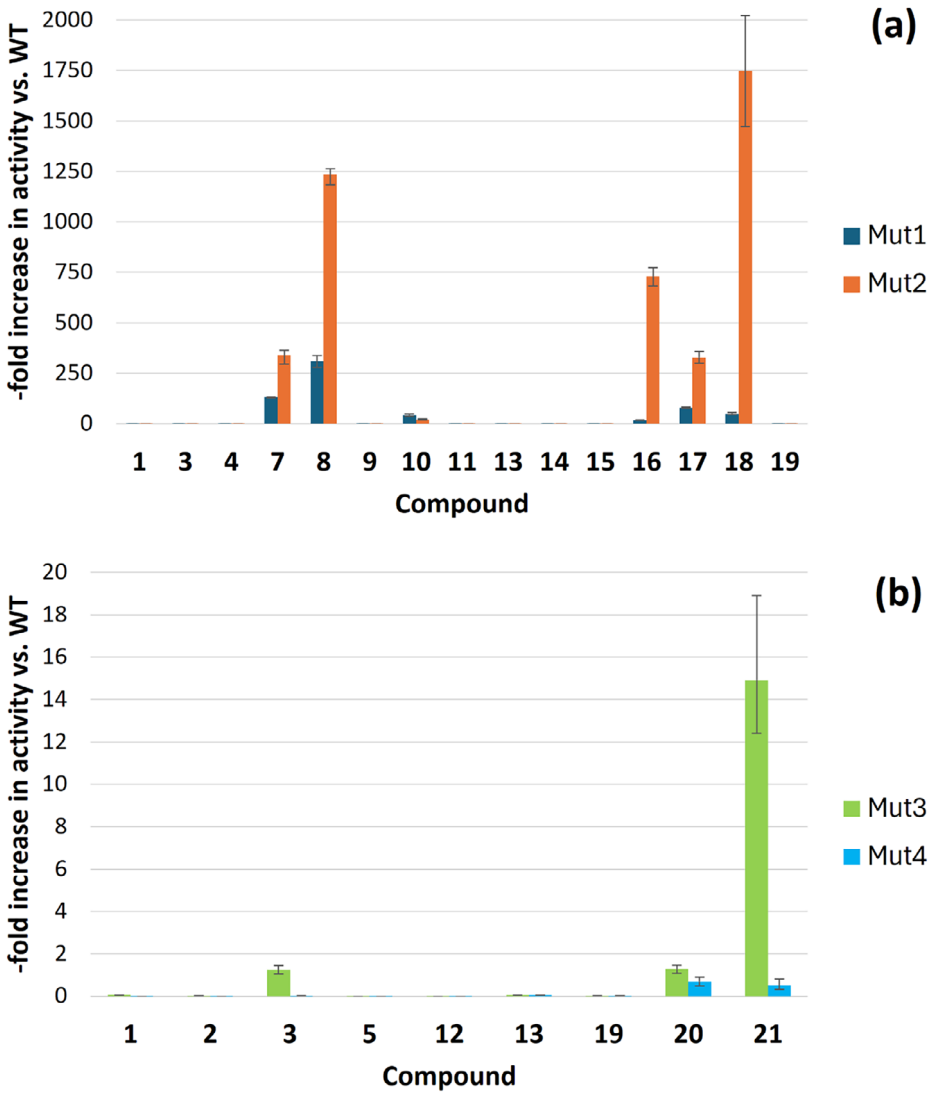

FIGURE 5 | Increase in activities of the *Pc*QueD variants by x-fold relative to the activity of the wild-type enzyme (WT) for the tested compounds **1**–**21**. (a) Mut1 and Mut2. (b) Mut3 and Mut4. Substrate concentrations in the aerated reaction mixtures were 30 μM, except for compounds **2** (10 μM), **3** (15 μM), **5** (14 μM), and **20** (15 μM).

pocket showed a 15-fold higher activity toward the smaller flavonol 3,7-dihydroxyflavone. Our results and the straightforward procedure described here have implications for engineering metalloenzymes to alter their substrate specificity toward novel compounds.

4 | Experimental Section

4.1 | Materials

Quercetin (compound **1**), galangin (**3**), fisetin (**5**), HEPES, and MES were obtained from Merck Life Science spol. s.r.o. (Prague, Czech Republic). Kaempferol (**2**) and myricetin (**4**) were purchased from abcr GmbH (Karlsruhe, Germany). Morin (**6**) was a product of Biosynth s.r.o. (Bratislava, Slovakia). All other flavonols, that is 8-phenyl quercetin (**7**), 8-(4-fluorophenyl) quercetin (**8**), 8-allyl quercetin (**9**), 8-(3-aminophenyl) quercetin (**10**), gossypetin (**11**), 3,3′,4′-trihydroxyflavone (**12**), 3,3′,4′,5′-tetrahydroxyflavone (**13**), 8-bromo quercetin (**14**), 6,8-dibromo quercetin (**15**), 8-(4-fluoroanilino) quercetin (**16**), 8-(4-methoxyanilino) quercetin (**17**), 8-(anilino) quercetin (**18**), 3′,4′-dimethoxyflavone (**19**), 3-hydroxyflavone (**20**), 7-hydroxyflavone (**21**), were prepared according to previously published methods [5, 43–47].

4.2 | Cloning and Mutagenesis of the *Pc*QueD-Encoding Gene

The in-gel digestion of protein bands and subsequent mass spectrometry of the tryptic peptides were performed as previously described [48]. Chromosomal DNA and total RNA were isolated from freeze-dried *Penicillium chrysogenum* CCF 1269 biomass using the RNA PowerSoil Total RNA Isolation Kit (Mo Bio Laboratories, Inc., USA) [33]. Amplification with degenerate primers was performed using Herculase hot start DNA polymerase (Agilent Technologies, Inc., USA). Amplification with specific primers was performed using Q5 hot start high-fidelity DNA polymerase (New England Biolabs) (Table S2). For cDNA

synthesis, reverse transcriptase from a second-generation 5′/3′ RACE kit (Roche) and a specific primer were used (Table S2). The cDNA-derived *Pc*QueD-encoding gene without its predicted signal sequence was then amplified and inserted into the pPICZα A vector downstream of the α-factor signal sequence encoded by the vector (Thermo Fisher Scientific Inc.; Table S2).

Mutagenesis of the *Pc*QueD-encoding gene was performed using either the QuikChange Lightning Multi Site-Directed Mutagenesis Kit or the QuikChange Lightning Site-Directed Mutagenesis Kit (Agilent Technologies, Santa Clara, CA, USA). The company's web-based tool was used for primer design (Table S14). The mutated *Pc*QueD-encoding DNA sequences were verified by sequencing both DNA strands.

4.3 | Heterologous Expression and Purification

Prior to electroporation of *Pichia pastoris* KM71H cells (Thermo Fisher Scientific Inc.) with 5–10 µg of plasmid DNA using a MicroPulser (Bio-Rad Laboratories, Inc., USA), the *Pc*QueD-encoding pPICZα A-based construct was linearized with PmeI. The resulting transformants were plated on YPD agar plates containing 0.5–1.0 mg mL^{-1} zeocin (InvivoGen Europe, France). Transformants were screened in liquid cultures using BMGY and BMM media with 0.5% methanol as inducer as previously described [48]. The BMM medium (30 mL per 300-mL baffled flask) contained 30 µM $CuSO_4$. The transformant with the highest *Pc*QueD production, determined by SDS-PAGE analysis of culture supernatants, was selected for preparative cultivation in BMGY/BMM media, with the latter supplemented with 30 µM $CuSO_4$.

After cultivation, the pH of the *Pc*QueD-containing culture supernatant was adjusted to 6.8 and loaded on 1-ml His-Trap FF columns (Merck Life Science spol. s.r.o., Czech Republic) equilibrated with binding buffer (20 mM phosphate, pH 7.4; 500 mM NaCl). Bound *Pc*QueD was eluted with a linear gradient of imidazole from 0 to 0.5 M.

The purified proteins were buffer-exchanged using Amicon Ultra-15 centrifugal filters (10 kDa cutoff; Merck Life Science spol. s.r.o., Czech Republic). Protein concentrations were determined at 280 nm with a DS 11 Series spectrophotometer (DeNovix Inc., USA) using the theoretical extinction coefficients.

4.4 | Deglycosylation

Deglycosylation of *Pc*QueD was performed according to the manufacturer's protocols using PNGase F (New England Biolabs).

4.5 | Reconstitution of Apo-*Pc*QueD

The in vitro reconstitution of wild-type *Pc*QueD involved chelating protein-bound metals with a 20-fold excess of both ethylenediaminetetraacetic acid (EDTA) and diethyl dithiocarbamate (DDTC) in 50 mM Tris-HCl (pH 7.4) on ice for 45 min. This was followed by dialysis in 20 mM HEPES (pH 7.4) for 24 h at 8°C and ultrafiltration using Amicon Ultra-15 (Ultracel-10k) centrifugal filter units (Merck Life Science spol. s.r.o., Czech Republic). Apo-*Pc*QueD was then incubated on ice with a 100-fold molar excess of a transition metal, followed by extensive ultrafiltration to remove unbound metal ions.

4.6 | Activity Determination and Steady-State Enzyme Kinetics

Enzyme activities were determined spectrophotometrically and by thin-layer chromatography (TLC). For TLC analysis of the reaction products, the enzymatic reactions were performed in a total volume of 120 µL with 20 µL of *P. pastoris* culture supernatant in 50 mM MES (pH 5.5) in the presence of 5 mM flavonol and 7% dimethyl sulfoxide using a Thermomixer (30°C, 800 rpm; Eppendorf Czech & Slovakia s.r.o.). The mobile phase was either ethyl acetate–2-propanol–water (3:2:2) or chloroform–acetone–formic acid (2:1:0.1) using silica gel 60 F_{254} plates (Merck KGaA). Steady-state enzyme activities were determined in 50 mM MES (pH 5.5; aerated [268 µM O_2] or O_2-saturated [1.37 mM O_2] [49]) at 22°C in the presence of 3% dimethyl sulfoxide using purified enzymes and a Shimadzu UV-1700 PharmaSpec spectrophotometer, monitoring the time-dependent decrease of the absorbance at 367 nm. For each substrate, the corresponding extinction coefficient was determined (Table S15). The web-based nonlinear regression program MyCurveFit was used for determining the apparent Michaelis-Menten kinetic parameters.

The pH dependence of the QueD activity was determined with **1** as a substrate and purified buffer-exchanged QueD. The following buffers (50 mM) were used: sodium citrate (pH 2.5–5.5), MES (pH 5.5 and 6.5), and HEPES (pH 7.5 and 8.2).

4.7 | Thermostabilities

Thermal stabilities of *Pc*QueD and its variants were determined by (1) analyzing residual enzymatic activities after a 10-min incubation at selected temperatures between 30 and 70°C, and (2) measuring fluorescence intensity at 330 and 350 nm with an excitation wavelength of 280 nm while continuously heating the protein sample at 1.0°C per minute (nanoDSF; Prometheus NT.48; NanoTemper Technologies GmbH, Germany).

4.8 | Circular Dichroism

Far and near-UV CD spectra were recorded with a Chirascan-plus CD spectrometer (Applied Photophysics Ltd., UK) at room temperature in 10 mM phosphate (pH 6.5) and 50 mM HEPES (pH 7.5) buffers, respectively. Far-UV CD measurements were performed in 1-mm cuvettes with protein concentrations of 0.13–0.15 mg mL^{-1}, whereas 1-cm cuvettes and protein concentrations of 0.18–0.50 mg mL^{-1} were used for the near-UV CD measurements. The secondary structure contents were estimated using the far-UV CD data and the CDNN software package.

4.9 | Inductively Coupled Plasma Mass Spectrometry

The metal contents in recombinant wild-type native *Pc*QueD after purification were determined using an Agilent 8900 inductively coupled plasma mass spectrometer (ICP-MS). The determination was performed in single quadrupole mode with helium gas in the collision cell (4.1 mL min^{-1}) using external calibration functions. The monitored isotopes were ^{55}Mn, ^{56}Fe, ^{59}Co, ^{60}Ni, ^{63}Cu, ^{66}Zn, ^{111}Cd, and ^{103}Rh, with ^{103}Rh serving as the internal standard. Before analysis, the protein samples were washed eight times with approximately seven volumes of 25 mM HEPES (pH 7.4) per wash using Amicon Ultra-0.5 centrifugal filters (10 kDa cutoff; Merck Life Science spol. s.r.o., Czech Republic). The samples were then prepared in 0.2% (m v^{-1}) HNO_3 for analysis. The metal content in the buffer solution was negligible.

4.10 | Large-Scale Biotransformation

The reaction mixture contained 10 mM **1**, 4.4 mL recombinant *P. pastoris* culture supernatant and 10% dimethyl sulfoxide in 25 mM HEPES (pH 7.5) in a total volume of 26 mL. After 24 h of shaking at 30°C, the reaction mixture was placed on ice and acidified to pH 2.1 with ice-cold HCl. The reaction product was extracted with an equal volume of ethyl acetate, and the organic phase was dried over Na_2SO_4, filtered, and evaporated *in vacuo*. The dry residue was dissolved in CD_3OD for NMR analysis.

4.11 | Analyses of Enzymatic Reaction Products

A Bruker Avance III HD spectrometer (^1H, 600 MHz; ^{13}C, 151 MHz) was used for NMR analysis. HPLC analyses were performed on a Shimadzu Prominence LC analytical system using a Chromolith RP-18e reversed-phase column (100 × 3 mm, Merck, Germany) (Figure S26). Reaction samples were analyzed by electrospray ionization mass spectrometry (ESI-MS) as described in Figure S26.

4.12 | Enzymatic Release of Carbon Monoxide

Compound **1**, unlabeled or ^{13}C-labeled at position C-3 [47], was used as the substrate for the *Pc*QueD-based reaction. The reaction mixture (30 μM **1**, 800 ng mL^{-1} purified *Pc*QueD, and 13% dimethyl sulfoxide in aerated 25 mM HEPES (pH 7.5) buffer; total volume of 800 μL) was placed in sealed GC vials fitted with PTFE septa, and the samples were left reacting for a given time at 22°C. The amount of released CO was determined by headspace sampling using a GC equipped with a TIC/MS detector operating in SIM mode and a PLOT CP-Molsieve 5Å GC column (30 m length, 0.53 mm inner diameter and 50 μm film thickness; Agilent J&W). The instrument was calibrated as described in Ramundo and coworkers (Figure S28) [47].

4.13 | Mass Photometry

A TwoMP mass photometer (Refeyn Ltd., UK) was used with precleaned glass coverslips. A silicon spacer (Grace Bio-Labs, USA) was placed on the glass surface to create wells for sample loading. The experiments were initiated with a drop of 18 μL of 50 mM citrate buffer containing 150 mM NaCl (pH 4.5), to which 2 μL of purified protein was added, resulting in a final protein concentration of 10 nM. Immediately after mixing, data were collected using AcquireMP with an acquisition time of 60 s. Calibration proteins were bovine serum albumin and IgG (Merck Life Science spol. s.r.o., Czech Republic). Protein masses were estimated by fitting the mass histograms to Gaussian functions (DiscoverMP software).

4.14 | Protein Model Construction and Molecular Docking

Sequence logos were generated with the online server WebLogo 3 [50] based on a multiple sequence alignment constructed by CLUSTAL W [51] as part of the BioEdit software [52]. Enzyme model structures were obtained using the AlphaFold 3 server [35]. Of the five generated models, those with different amino acid rotamers within 3.0 Å of bound compound **1** (position determined from the X-ray structure with the pdb accession code 1h1i) [14] were selected as representatives for docking analysis. For molecular docking, the compounds were prepared in YASARA, which was also used for structural alignments of proteins and molecular dynamics simulations (without including the C-terminal His-tag of *Pc*QueD) using the standard protocol (Yamber3 force field and NPT ensemble, 298 K and 1 bar, 100 ns) [53, 54]. The structure of compound **1** was downloaded from the PubChem database [55]. The software PLANTS was used for molecular docking [56, 57]. Docking poses were scored with the empirical scoring function CHEMPLP. The scores were reported as average values. Electrostatic potentials were calculated with Gaussian 16 and visualized using VMD. PoseView was used for 2D visualization of enzyme-ligand interactions [58].

Acknowledgments

We thank Jana Fritschková and Adéla Kovaříčková for their assistance with cultivations and gel electrophoresis. We also thank Prof. Petr Klán for the opportunity to conduct the carbon monoxide release experiments in his laboratory. This work was supported by the Czech Science Foundation (grant no. 23-04654S), the Czech Academy of Sciences (Institutional Research Plan RVO: 68081715), and the Ministry of Education, Youth and Sports of the Czech Republic (grant nos. LUC23061, LUC25026, LM2023042, and CZ.02.01.01/00/22_008/0004597). The CD and DSF data were recorded at the core facility Biophysical techniques at CMS/CIISB, Instruct-CZ Centre (Biocev), supported by the European Regional Development Fund-Project „UP CIISB" (grant no. CZ.02.1.01/0.0/0.0/18_046/0015974). Computational resources were provided by the e-INFRA CZ project (ID 90254), supported by the Ministry of Education, Youth and Sports of the Czech Republic, and the ELIXIR-CZ project (ID 90255), part of the international ELIXIR infrastructure.

Conflicts of Interest

The authors declare no conflicts of interest.

Data Availability Statement

The data that support the findings of this study are available in the supplementary material of this article.

References

1. M. Kotik, N. Kulik, and K. Valentová, "Flavonoids as Aglycones in Retaining Glycosidase-catalyzed Reactions: Prospects for Green Chemistry," *Journal of Agricultural and Food Chemistry* 71 (2023): 14890–14910, https://doi.org/10.1021/acs.jafc.3c04389.

2. S. Tranchimand, P. Brouant, and G. Iacazio, "The Rutin Catabolic Pathway with Special Emphasis on Quercetinase," *Biodegradation* 21 (2010): 833–859, https://doi.org/10.1007/s10532-010-9359-7.

3. A. V. A. David, R. Arulmoli, and S. Parasuraman, "Overviews of Biological Importance of Quercetin: A Bioactive Flavonoid," *Pharmacognosy Reviews* 10 (2016): 84, https://doi.org/10.4103/0973-7847.194044.

4. T. L. A. Nguyen and D. Bhattacharya, "Antimicrobial Activity of Quercetin: An Approach to Its Mechanistic Principle," *Molecules* 27 (2022): 2494, https://doi.org/10.3390/molecules27082494.

5. M. Hurtová, D. Brdová, B. Křížkovská, et al., "Nitrogen-Containing Flavonoids—Preparation and Biological Activity," *ACS Omega* 9 (2024): 34938–34950, https://doi.org/10.1021/acsomega.4c04627.

6. M. Monagas, M. Urpi-Sarda, F. Sánchez-Patán, et al., "Insights into the Metabolism and Microbial Biotransformation of Dietary Flavan-3-ols and the Bioactivity of Their Metabolites," *Food & Function* 1 (2010): 233, https://doi.org/10.1039/c0fo00132e.

7. A. F. Almeida, G. I. A. Borge, M. Piskula, et al., "Bioavailability of Quercetin in Humans With a Focus on Interindividual Variation," *Comprehensive Reviews in Food Science and Food Safety* 17 (2018): 714–731, https://doi.org/10.1111/1541-4337.12342.

8. C. N. dos Santos, R. Menezes, D. Carregosa, et al., "Flavonols and Flavones" in *Dietary Polyphenols: Their Metabolism and Health Effects* (ed.: F. A. Tomás-Barberán, A. González-Sarrías, R. García-Villalba), (John Wiley & Sons, Inc., 2020): 163–198.

9. A. Braune, "Flavonoid-converting Capabilities of *Clostridium butyricum*," *Applied Microbiology and Biotechnology* 109 (2025): 53, https://doi.org/10.1007/s00253-025-13434-0.

10. M. Adams and Z. Jia, "Structural and Biochemical Analysis Reveal Pirins to Possess Quercetinase Activity," *Journal of Biological Chemistry* 280 (2005): 28675–28682, https://doi.org/10.1074/jbc.M501034200.

11. B. Guo, Y. Zhang, G. Hicks, et al., "Structure-dependent Modulation of Substrate Binding and Biodegradation Activity of Pirin Proteins toward Plant Flavonols," *ACS Chemical Biology* 14 (2019): 2629–2640, https://doi.org/10.1021/acschembio.9b00575.

12. F. Fusetti, K. H. Schröter, and R. A. Steiner, "Crystal Structure of the Copper-Containing Quercetin 2,3-dioxygenase From *Aspergillus japonicus*," *Structure (London, England)* 10 (2002): 259–268, https://doi.org/10.1016/S0969-2126(02)00704-9.

13. B. Gopal, L. L. Madan, S. F. Betz, and A. A. Kossiakoff, "The Crystal Structure of a Quercetin 2,3-dioxygenase from *Bacillus subtilis* Suggests Modulation of Enzyme Activity by a Change in the Metal Ion at the Active Site(s)," *Biochemistry* 44 (2005): 193–201, https://doi.org/10.1021/bi0484421.

14. R. A. Steiner, K. H. Kalk, and B. W. Dijkstra, "Anaerobic Enzyme·Substrate Structures Provide Insight into the Reaction Mechanism of the Copper-dependent Quercetin 2,3-dioxygenase," *Proceedings of the National Academy of Sciences* 99 (2002): 16625–16630, https://doi.org/10.1073/pnas.262506299.

15. R. A. Steiner, W. Meyer-Klaucke, and B. W. Dijkstra, "Functional Analysis of the Copper-dependent Quercetin 2,3-dioxygenase. 2. X-ray Absorption Studies of Native Enzyme and anaerobic Complexes with the Substrates Quercetin and Myricetin," *Biochemistry* 41 (2002): 7963–7968, https://doi.org/10.1021/bi015974y.

16. R. A. Steiner, I. M. Kooter, and B. W. Dijkstra, "Functional Analysis of the Copper-Dependent Quercetin 2,3-Dioxygenase. 1. Ligand-Induced Coordination Changes Probed by X-ray Crystallography: Inhibition, Ordering Effect, and Mechanistic Insights," *Biochemistry* 41 (2002): 7955–7962, https://doi.org/10.1021/bi0159736.

17. M. R. Schaab, B. M. Barney, and W. A. Francisco, "Kinetic and Spectroscopic Studies on the Quercetin 2,3-Dioxygenase From *Bacillus subtilis*," *Biochemistry* 45 (2006): 1009–1016, https://doi.org/10.1021/bi051571c.

18. S. Fetzner, "Ring-Cleaving Dioxygenases with a Cupin Fold," *Applied and Environmental Microbiology* 78 (2012): 2505–2514, https://doi.org/10.1128/AEM.07651-11.

19. J. Chen, W. Li, and M. Wang, et al., "Crystal Structure and Mutagenic Analysis of GDOsp, a Gentisate 1,2-Dioxygenase From *Silicibacter pomeroyi*," *Protein Science* 17 (2008): 1362–1373, https://doi.org/10.1110/ps.035881.108.

20. M. Ferraroni, I. Matera, and S. Bürger, et al., "The Salicylate 1,2-Dioxygenase as a Model for a Conventional Gentisate 1,2-Dioxygenase: Crystal Structures of the G106A Mutant and Its Adducts with Gentisate and Salicylate," *The FEBS Journal* 280 (2013): 1643–1652, https://doi.org/10.1111/febs.12173.

21. J. Yang, Y.-Z. Xiao, R. Li, Y. Liu, and L.-J. Long, "Repurposing a Bacterial Prolidase for Organophosphorus Hydrolysis: Reshaped Catalytic Cavity Switches Substrate Selectivity," *Biotechnology and Bioengineering* 117 (2020): 2694–2702, https://doi.org/10.1002/bit.27455.

22. J. Büchler, S. Honda Malca, D. Patsch, et al., "Algorithm-Aided Engineering of Aliphatic Halogenase WelO5* for the Asymmetric Late-stage Functionalization of Soraphens," *Nature Communications* 13 (2022): 371, https://doi.org/10.1038/s41467-022-27999-1.

23. Z. Zhang, M. Long, N. Zheng, et al., "Redesign of γ-Glutamyl Transpeptidase From *Bacillus subtilis* for High-level Production of L-Theanine by Cavity Topology Engineering," *Applied Microbiology and Biotechnology* 107 (2023): 3551, https://doi.org/10.1007/s00253-023-12544-x.

24. Z. Zhang, M. Long, N. Zheng, et al., "Inside Out Computational Redesign of Cavities for Improving Thermostability and Catalytic Activity of *Rhizomucor miehei* Lipase," *Applied and Environmental Microbiology* 89 (2023): e02172–22, https://doi.org/10.1128/aem.02172-22.

25. J. Niu, B. Ma, J. Shen, et al., "Structure-guided Steric Hindrance Engineering of *Devosia* Strain A6−243 Quinone-Dependent Dehydrogenase to Enhance Its Catalytic Efficiency," *Journal of Agricultural and Food Chemistry* 72 (2024): 549, https://doi.org/10.1021/acs.jafc.3c07179.

26. S. C. L. Kamerlin and A. Warshel, "At the Dawn of the 21st Century: Is Dynamics the Missing Link for Understanding Enzyme Catalysis?," *Proteins: Structure, Function, and Bioinformatics* 78 (2010): 1339–1375, https://doi.org/10.1002/prot.22654.

27. N. G. Nezhad, R. N. Z. R. Abd Rahman, M. Yahaya, et al., "Recent Advances in Simultaneous Thermostability-Activity Improvement of Industrial Enzymes Through Structure Modification," *International Journal of Biological Macromolecules* 232 (2023): 123440, https://doi.org/10.1016/j.ijbiomac.2023.123440.

28. R. Sun, D. Wu, P. Chen, and P. Zheng, "Cutting-Edge Computational Approaches in Enzyme Design and Activity Enhancement," *Biochemical Engineering Journal* 212 (2024): 109510, https://doi.org/10.1016/j.bej.2024.109510.

29. A. R. Nazmi, M. Muralidharan, and G. Lloyd-Jones, "Manipulating Intradiol Dioxygenases by C-Terminus Truncation," *Enzyme and Microbial Technology* 125 (2019): 21–28, https://doi.org/10.1016/j.enzmictec.2019.02.007.

30. R. Caglio, F. Valetti, P. Caposio, G. Gribaudo, E. Pessione, and C. Giunta, "Fine-Tuning of Catalytic Properties of Catechol 1,2-Dioxygenase by Active Site Tailoring," *Chembiochem* 10 (2009): 1015–1024, https://doi.org/10.1002/cbic.200800836.

31. E. Eppinger and A. Stolz, "Expansion of the Substrate Range of the Gentisate 1,2-Dioxygenase From *Corynebacterium glutamicum* for the Conversion of Monohydroxylated Benzoates," *Protein Engineering, Design and Selection* 30 (2017): 57, https://doi.org/10.1093/protein/gzw061.

32. H. Eom, Y. Cao, H. Kim, S. P. de Visser, and W. J. Song, "Underlying Role of Hydrophobic Environments in Tuning Metal Elements for

Efficient Enzyme Catalysis," *Journal of the American Chemical Society* 145 (2023): 5880–5887, https://doi.org/10.1021/jacs.2c13337.

33. M. Kotik, K. Brodsky, P. Halada, et al., "Access to Both Anomers of Rutinosyl Azide Using Wild-Type Rutinosidase and Its Catalytic Nucleophile Mutant," *Catalysis Communications* 149 (2021): 106193, https://doi.org/10.1016/j.catcom.2020.106193.

34. S. Tranchimand, G. Ertel, V. Gaydou, C. Gaudin, T. Tron, and G. Iacazio, "Biochemical and Molecular Characterization of a Quercetinase From *Penicillium olsonii*," *Biochimie* 90 (2008): 781–789, https://doi.org/10.1016/j.biochi.2007.12.004.

35. J. Abramson, J. Adler, J. Dunger, et al., "Accurate Structure Prediction of Biomolecular Interactions with AlphaFold 3," *Nature* 630 (2024): 493, https://doi.org/10.1038/s41586-024-07487-w.

36. F. J. Simpson, G. Talbot, and D. W. S. Westlake, "Production of Carbon Monoxide in the Enzymatic Degradation of Rutin," *Biochemical and Biophysical Research Communications* 2 (1960): 15–18, https://doi.org/10.1016/0006-291X(60)90255-2.

37. F. J. Simpson, N. Narasimhachari, and D. W. S. Westlake, "Degradation of Rutin by *Aspergillus flavus*: the Carbon Monoxide Producing System," *Canadian Journal of Microbiology* 9 (1963): 15, https://doi.org/10.1139/m63-002.

38. H. Bisswanger, *Enzyme Kinetics: Principles and Methods* (WILEY-VCH Verlag GmbH & Co. KGaA, 2008): 120–121, https://doi.org/10.1002/9783527622023.

39. S. Tranchimand, T. Tron, C. Gaudin, and G. Iacazio, "First Chemical Synthesis of Three Natural Depsides Involved in Flavonol Catabolism and Related to Quercetinase Catalysis," *Synthetic Communications* 36 (2006): 587–597, https://doi.org/10.1080/00397910500406534.

40. R. J. Simpson, *Proteins and Proteomics: A Laboratory Manual* (Cold Spring Harbor Laboratory Press, 2003).

41. A. Fersht, *Enzyme Structure and Mechanism*, Second Edition (W. H. Freeman and Company, 2008): 324–327.

42. J. Gao, S. Ma, D. T. Major, K. Nam, J. Pu, and D. G. Truhlar, "Mechanisms and Free Energies of Enzymatic Reactions," *Chemical Reviews* 106 (2006): 3188–3209, https://doi.org/10.1021/cr050293k.

43. R. G. Britton, E. Horner-Glister, O. A. Pomenya, et al., "Synthesis and Biological Evaluation of Novel Flavonols as Potential Anti-Prostate Cancer Agents," *European Journal of Medicinal Chemistry* 54 (2012): 952–958, https://doi.org/10.1016/j.ejmech.2012.06.031.

44. X. Li, G. Chen, X. Zhang, et al., "A New Class of Flavonol-based Anti-prostate Cancer Agents: Design, Synthesis, and Evaluation in Cell Models," *Bioorganic & Medicinal Chemistry Letters* 26 (2016): 4241–4245, https://doi.org/10.1016/j.bmcl.2016.07.050.

45. M. Hurtová, D. Biedermann, M. Kuzma, and V. Křen, "Mild and Selective Method of Bromination of Flavonoids," *Journal of Natural Products* 83 (2020): 3324–3331, https://doi.org/10.1021/acs.jnatprod.0c00655.

46. M. Hurtová, D. Biedermann, Z. Osifová, J. Cvačka, K. Valentová, and V. Křen, "Preparation of Synthetic and Natural Derivatives of Flavonoids Using Suzuki–Miyaura Cross-Coupling Reaction," *Molecules* 27 (2022): 967, https://doi.org/10.3390/molecules27030967.

47. A. Ramundo, M. Hurtová, I. Božek, et al., "Multimodal Carbon Monoxide Photorelease From Flavonoids," *Organic Letters* 26 (2024): 708–712, https://doi.org/10.1021/acs.orglett.3c04141.

48. D. Šimčíková, M. Kotik, L. Weignerová, et al., "α-L-Rhamnosyl-β-D-Glucosidase (rutinosidase) From *Aspergillus niger*: Characterization and Synthetic Potential of a Novel Diglycosidase," *Advanced Synthesis & Catalysis* 357 (2015): 107, https://doi.org/10.1002/adsc.201400566.

49. A. J. Fielding, E. G. Kovaleva, E. R. Farquhar, J. D. Lipscomb, and L. Que Jr, "A Hyperactive Cobalt-Substituted Extradiol-Cleaving Catechol Dioxygenase," *Journal of Biological Inorganic Chemistry* 16 (2011): 341–355, https://doi.org/10.1007/s00775-010-0732-0.

50. G. E. Crooks, G. Hon, J. M. Chandonia, and S. E. Brenner, "WebLogo: a Sequence Logo Generator," *Genome Research* 14 (2004): 1188–1190, https://doi.org/10.1101/gr.849004.

51. J. D. Thompson, D. G. Higgins, and T. J. Gibson, "CLUSTAL W: Improving the Sensitivity of Progressive Multiple Sequence Alignment Through Sequence Weighting, Position-Specific Gap Penalties and Weight Matrix Choice," *Nucleic Acids Research* 22 (1994): 4673–4680, https://doi.org/10.1093/nar/22.22.4673.

52. T. A. Hall, "BioEdit: A User-Friendly Biological Sequence Alignment Editor and Analysis Program for Windows 95/98/NT," *Nucleic Acids Symposium Series* 41 (1999): 95–98.

53. E. Krieger, R. L. Dunbrack Jr., R. W. Hooft, and B. Krieger, "Assignment of Protonation States in Proteins and Ligands: Combining pKa Prediction with Hydrogen Bonding Network Optimization," *Methods in Molecular Biology* 819 (2012): 405–421, https://doi.org/10.1007/978-1-61779-465-0_25.

54. E. Krieger and G. Vriend, "YASARA View—Molecular Graphics for all Devices—From Smartphones to Workstations," *Bioinformatics* 30 (2014): 2981–2982, https://doi.org/10.1093/bioinformatics/btu426.

55. S. Kim, J. Chen, T. Cheng, et al., "PubChem 2025 Update," *Nucleic Acids Research* 53 (2025): D1516–D1525, https://doi.org/10.1093/nar/gkae1059.

56. O. Korb, T. Stützle, and E. T. Exner in *Ant Colony Optimization and Swarm Intelligence. ANTS 2006. Lecture Notes in Computer Science*, 4150 (ed.: M. Dorigo, L. M. Gambardella, M. Birattari, A. Martinoli, R. Poli, T. Stützle), (Springer, 2006): 247–258.

57. S. C. Süleyman and E. Timucin, "Comparative Assessment of Seven Docking Programs on a Nonredundant Metalloprotein Subset of the PDBbind Refined," *Journal of Chemical Information and Modeling* 59 (2019): 3846–3859, https://doi.org/10.1021/acs.jcim.9b00346.

58. K. Stierand and M. Rarey, "Drawing the PDB: Protein–Ligand Complexes in Two Dimensions," *ACS Medicinal Chemistry Letters* 1 (2010): 540–545, https://doi.org/10.1021/ml100164p.

59. T. N. Petersen, S. Brunak, G. von Heijne, and H. Nielsen, "SignalP 4.0: Discriminating Signal Peptides from Transmembrane Regions," *Nature Methods* 8 (2011): 785–786, https://doi.org/10.1038/nmeth.1701.

Supporting Information

Additional supporting information can be found online in the Supporting Information section.

The authors have cited an additional reference within the Supporting Information [59].

Supporting File: cctc70670-sup-0001-SuppMat.pdf.